# Interband effects in the $c$-axis optical conductivity in $YBa_2Cu_3O_{7-\delta}$

W. A. Atkinson* and J. P. Carbotte
*Department of Physics and Astronomy, McMaster University, Hamilton, Ontario, Canada L8S 4M1*
(Received 27 August 1996)

The normal state optical conductivity is calculated for a layered metal with two layers per unit cell coupled through a transverse hopping matrix element $t_\perp$. The optical response involves an interband term in addition to the more familiar intraband term which leads to the usual Drude form. The interband term is only weakly temperature dependent, even for an inelastic scattering rate which is linear in $T$. It gives a $c$-axis response which extends in frequency over the entire bandwidth, although there can be structure on this energy scale which reflects details of the electronic structure. In particular, at low energy, the $c$-axis response can develop a gap or pseudogap as the temperature is lowered. At high temperature, a Drude response will be seen only if the intraband transitions, which are of order $t_\perp^4$, become important compared with the interband transitions which are of order $t_\perp^2$ [S0163-1829(97)00905-3]

## I. INTRODUCTION

Models of the high-$T_c$ oxides often start with a single isolated $CuO_2$ layer. Other structural elements within the unit cell are usually labeled as charge reservoirs or barrier layers and are ignored. Yet it is precisely the nature of the coupling between the different layers that determines $c$-axis transport properties, which are found to display a rich variety of behaviors and are often anomalous.[1,2] The anomalous nature of the $c$-axis conductivity has been variously interpreted as suggesting that interlayer coupling is an essential piece of the superconducting mechanism,[3] that the interlayer coupling is incoherent due to impurity or phononic scattering[4–7] or thermal fluctuations,[8] or that the $CuO_2$ layers are in a non-Fermi-liquid state.[9] In this work, we suggest that the $c$-axis optical conductivity in $YBa_2Cu_3O_{7-\delta}$ ($YBCO_{7-\delta}$) can be explained by proper consideration of the multilayered structure of the unit cell.

In considering $c$-axis properties, it is important to distinguish between the coupling between various conducting layers within a unit cell (which can contain several planes) and the intercell coupling which could involve some barrier layer. It is this latter coupling that probably governs the size of the anisotropy observed between $c$-axis[1,2,10–12] and $ab$-plane properties. On the other hand, the large in-plane anisotropy between $a$ and $b$ directions[13–17] (along the CuO chains) observed in YBCO is related more closely to the properties within a unit cell. The actual situation is clearly quite complex. For example, the unit cell in YBCO consists of a bilayer of two $CuO_2$ planes separated by a CuO chain layer. In addition, the chains are only completed in $YBa_2Cu_3O_7$ and the effect of oxygen doping on the chain Fermi surface is not well understood and neither is the partition of holes between planes and chains. Because of these uncertainties, it is necessary, at this stage, to use a simplified model and to set specific but limited aims.

Having recognized that several distinct transverse hopping matrix elements come into a complete description of the $c$-axis properties of the oxides, we will, nevertheless, limit ourselves here to a model of two layers per unit cell coupled through a single transverse matrix element $t_\perp$. With YBCO in mind, one of the two layers will be assumed to have tetragonal symmetry and model a $CuO_2$ plane, while the other will be taken to have orthorhombic symmetry and represent a CuO chain. While this model is admittedly crude, it does allow us to examine the role of interband transitions on the optical conductivity. We are interested in addressing two questions: What is the magnitude of the interband contribution to the conductivity compared to the intraband (or Drude) contribtuion, and how different is the frequency dependence of the interband contribution from that of the Drude contribution?

Not surprisingly, we find that the interband contributions are of order $t_\perp^2$ and are therefore relatively unimportant for the $a$- and $b$-axis optical conductivities. On the other hand, the results are reversed for the $c$-axis conductivity: The interband contributions are of order $t_\perp^2$ and dominate the intraband contributions—which are of order $t_\perp^4$—for weak interlayer couplings. It is not surprising, then, that the $c$-axis conductivity should have a non-Drude frequency dependence. In the work which follows, we will examine this frequency dependence and compare it with experiment.

The paper is structured as follows. In Sec. II, general expressions for the optical conductivity of a system with two layers per unit cell are derived. In Sec. III a specific model (the plane-chain model) which is suitable for YBCO is introduced. Numerical results are given for the conductivity which we present separately for $a$, $b$ (along the chains), and $c$ (perpendicular to the planes) directions. In Sec. IV, the expression for the conductivity derived in the previous section is reduced analytically, with the intention of highlighting the two types of contribution (interband and intraband) to the conductivity. One of the important results of this section is to show how the different contributions to the conductivity depend on the chain-plane coupling $t_\perp$. In Sec. V, expressions for the conductivity in the case of a bilayer—consisting of two identical but unevenly spaced planes in each unit cell—are derived. The calculation is interesting because YBCO, as well as many other cuprate superconductors, contains a $CuO_2$ bilayer in the unit cell. One of our main conclusions in

 

this section is that the coupling between the $CuO_2$ planes is not as likely to be the source of the broad background seen in the $c$-axis optical conductivity as is the coupling between the $CuO_2$ planes and the chains. Section VI consists of a short discussion of sum rules. A long conclusion, which includes some further discussion and a summary, is to be found in the final section.

## II. CONDUCTIVITY IN A LAYERED SYSTEM

The purpose of this section is to derive the equations needed for our numerical calculations of the optical conductivity. In linear response theory, the real part of the conductivity tensor $\sigma_{\mu\nu}$ is related to the imaginary part of the current-current correlation function $\Pi_{\mu\nu}$ by[18]

$$\mathrm{Re}[\sigma_{\mu\nu}(\omega)]=\frac{2}{\omega}\mathrm{Im}[\Pi_{\mu\nu}(\omega)], \tag{1}$$

where the Greek subscripts refer to spatial components and $\omega$ is the frequency. The factor of 2 is to account for electron spins, which will otherwise be ignored for the rest of this article. In the superconducting state, the spins are dealt with explicitly in the calculation of $\Pi(\omega)$. In a previous article we evaluated $\Pi$ for a two-layered tight binding system.[19] The intention of our earlier calculations was to find the penetration depth, so that $\Pi$ was evaluated at zero frequency ($\omega=0$) and in the superconducting state. Here we will evaluate $\Pi(\omega)$ at finite frequency and in the normal state. As before, the model is a two-layer tight binding model, so that the calculation is very similar to our earlier one. For this reason, the reader is referred to our earlier work for details of the calculation which are not shown here.

In previous work, we showed that[19]

$$\Pi_{\mu\nu}(i\nu_n)=e^2\frac{1}{\beta}\sum_m\frac{1}{\Omega}\sum_{\mathbf{k}}\mathrm{Tr}[G(\mathbf{k};i\omega_m-i\nu_n)\times\gamma_\mu(\mathbf{k},\mathbf{k})G(\mathbf{k};i\omega_m)\gamma_\nu(\mathbf{k},\mathbf{k})], \tag{2}$$

where $\nu_n$ and $\omega_m$ are the boson and fermion Matsubara frequencies, respectively, $G(\mathbf{k};i\omega_m)$ are the thermal Green's functions, and $\gamma_\mu$ are the electromagnetic vertex functions. This result is essentially the standard result,[18] with the exception that here the Green's functions and vertex functions are $2\times2$ matrices whose diagonal elements (e.g., $G_{11}$) describe properties of a single layer and whose off-diagonal elements describe the interlayer coupling. The trace in Eq. (2) is over the matrix product contained in the square brackets. In order to find the optical conductivity, we need to find explicit forms for $G$ and $\gamma_\mu$, and we begin by introducing our model for the two layer system.

The model we are going to present describes a metallic system with two types of layer stacked along the $c$ axis (or, equivalently, the $z$ axis). In Sec. III one of the layers is a two-dimensional plane layer, while the other is a one-dimensional chain layer. In Sec. V both layers are plane layers. We define the operators $c_{1\mathbf{k}}$ and $c_{2\mathbf{k}}$ to be the annihilation operators for the two types of layer. The wave vectors $\mathbf{k}$ are three dimensional. The Hamiltonian[19–21] for our model is

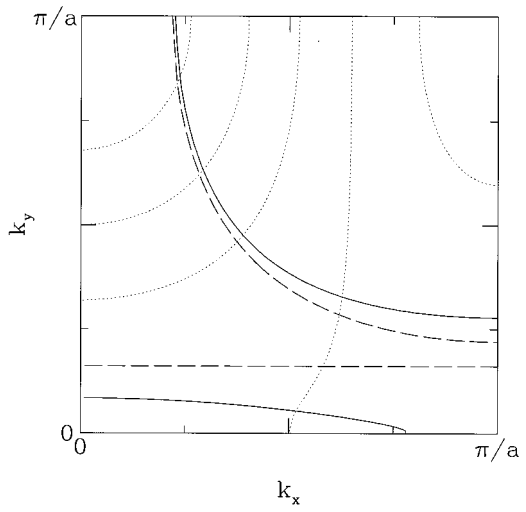


FIG. 1. Fermi surface for the chain-plane model. The Fermi surface is shown for $k_z=0$ (solid curve) and $k_z=\pi/d$ (dashed curve). When $k_z=\pi/d$, the chain-plane coupling $t(\mathbf{k})$ vanishes and the Fermi surface is that of the isolated chain and plane layers. The dotted curves are lines of the constant energy difference $\omega=\epsilon_+-\epsilon_-$. The band structure parameters chosen for this case are $\{t_1,t_2,\mu_1,\mu_2,t_\perp\}=\{70,100,-65,-175,20\}$ meV and $B=0.45$.

$$H=\sum_{\mathbf{k}}\begin{bmatrix}c_{1\mathbf{k}}^\dagger & c_{2\mathbf{k}}^\dagger\end{bmatrix}h(\mathbf{k})\begin{bmatrix}c_{1\mathbf{k}}\\ c_{2\mathbf{k}}\end{bmatrix}, \tag{3}$$

with

$$h(\mathbf{k})=\begin{bmatrix}\xi_1 & t\\ t^* & \xi_2\end{bmatrix}, \tag{4}$$

and where $\xi_1(\mathbf{k})$ and $\xi_2(\mathbf{k})$ are the energy dispersions for the two types of layer, and $t(\mathbf{k})$ connects the layers through single electron hopping. The specific forms of $\xi_1$, $\xi_2$, and $t$ will be given in Secs. III and V.

The Hamiltonian matrix $h(\mathbf{k})$ is diagonalized by the unitary matrices $U(\mathbf{k})$, so that

$$\begin{bmatrix}\epsilon_+(\mathbf{k}) & 0\\ 0 & \epsilon_-(\mathbf{k})\end{bmatrix}=U^\dagger(\mathbf{k})h(\mathbf{k})U(\mathbf{k}), \tag{5}$$

where

$$U(\mathbf{k})=\frac{1}{\sqrt{\epsilon_+-\epsilon_-}}\begin{bmatrix}-\frac{t}{|t|}\sqrt{\xi_1-\epsilon_-} & -\frac{t}{|t|}\sqrt{\epsilon_+-\xi_1}\\ -\sqrt{\epsilon_+-\xi_1} & \sqrt{\xi_1-\epsilon_-}\end{bmatrix}, \tag{6}$$

and where $\epsilon_\pm(\mathbf{k})$ are the eigenvalues of $h(\mathbf{k})$ [i.e., $\epsilon_\pm(\mathbf{k})$ are the band energies],

$$\epsilon_\pm=\frac{\xi_1+\xi_2}{2}\pm\sqrt{\left(\frac{\xi_1-\xi_2}{2}\right)^2+t^2}. \tag{7}$$

The Fermi surfaces are the solutions of the equations $\epsilon_\pm(\mathbf{k})=0$. As an example, one possible Fermi surface for the chain-plane system—which is discussed in more detail in Sec. III—is shown in Fig. 1.

The single-particle Green's function is determined from the Hamiltonian:

$$G(\mathbf{k};i\omega_n)^{-1}=\begin{bmatrix} i\omega_n-\xi_1 & -t \\ -t^* & i\omega_n-\xi_2 \end{bmatrix}. \tag{8}$$

If we wish to include impurity scattering, then the simplest approach is to introduce a scattering rate $\Gamma$:

$$G(\mathbf{k};i\omega_n)^{-1} = \begin{bmatrix} i\omega_n-\xi_1+i\Gamma\,\mathrm{sgn}(\omega_n) & -t \\ -t^* & i\omega_n-\xi_2+i\Gamma\,\mathrm{sgn}(\omega_n) \end{bmatrix}. \tag{9}$$

We will assume that $\Gamma$ is independent of frequency and momentum, but that it varies linearly with temperature as is observed in the copper oxides for the in-plane conductivity. At $T=0$, the system is in the clean limit ($\Gamma=0$), and at $T=100$ K, $\Gamma=10$ meV. The scattering rate is related to the quasiparticle lifetime by $\Gamma=\hbar/2\tau$.

Finally, we need to find the vertex function $\gamma_\mu(\mathbf{k},\mathbf{k})$. In previous work[19,22] it has been shown that in the tight binding model, $\gamma_\mu(\mathbf{k},\mathbf{k})$ is just the gradient of the Hamiltonian matrix in $\mathbf{k}$ space:

$$\gamma_\mu(\mathbf{k},\mathbf{k})=\frac{1}{\hbar}\frac{\partial}{\partial k_\mu}\begin{bmatrix} \xi_1 & t \\ t^* & \xi_2 \end{bmatrix}. \tag{10}$$

Equations (2), (9), and (10) are sufficient to calculate the optical conductivity. In their current form, however, they are not very revealing and it is difficult to understand the results of our numerical calculations without some further work. We will make two manipulations in order to make the formula for the conductivity more transparent. The first is to write the conductivity in terms of spectral functions, instead of Green's functions:

$$\mathrm{Re}[\sigma_{\mu\nu}(\omega)]=\frac{e^2\hbar}{2\pi\Omega}\sum_{\mathbf{k}}\int_{-\infty}^{\infty}dx\,\mathrm{Tr}[A(\mathbf{k};x)\gamma_\mu(\mathbf{k},\mathbf{k}) \times A(\mathbf{k};x+\hbar\omega)\gamma_\nu(\mathbf{k},\mathbf{k})]\frac{f(x)-f(x+\hbar\omega)}{\hbar\omega}, \tag{11}$$

where the spectral function $A(\mathbf{k};\omega)$ is defined by analytically continuing $G(\mathbf{k},i\omega_n)$ to the real axis,

$$A(\mathbf{k};\omega)=i[G(\mathbf{k};\omega+i0)-G(\mathbf{k};\omega-i0)],$$

and where $f(x)$ is the Fermi function.

The second manipulation is to make a change of basis, so that the eigenstates of the Hamiltonian, rather than the eigenstates of the isolated layers, are used as the basis states. In other words, we will evaluate

$$\mathrm{Re}[\sigma_{\mu\nu}(\omega)]=\frac{e^2\hbar}{2\pi\Omega}\sum_{\mathbf{k}}\int_{-\infty}^{\infty}dx\,\mathrm{Tr}[\hat{A}(\mathbf{k};x)\hat{\gamma}_\mu(\mathbf{k},\mathbf{k}) \times \hat{A}(\mathbf{k};x+\hbar\omega)\hat{\gamma}_\nu(\mathbf{k},\mathbf{k})]\frac{f(x)-f(x+\hbar\omega)}{\hbar\omega}, \tag{12}$$

where we introduce the notation, throughout this work, $\hat{O}(\mathbf{k})\equiv U^\dagger(\mathbf{k})O(\mathbf{k})U(\mathbf{k})$, with $O(\mathbf{k})$ a $2\times2$ matrix.

Equation (12) is more useful than Eq. (2) for two reasons. The first is that the spectral function has a simple interpretation as the density of states. The second is that $\hat{A}$ has a particularly simple form. The price we pay is that the vertex function $\hat{\gamma}_\mu$ is more complicated to evaluate than $\gamma_\mu$.

The vertex function $\hat{\gamma}_\mu$ can be found by explicitly performing the matrix multiplication $U^\dagger(\mathbf{k})\gamma_\mu U(\mathbf{k})$, and we will explore it in detail in the following sections. The spectral function can be evaluated easily here. In the new basis

$$\hat{G}(\mathbf{k};i\omega_n)^{-1} = \begin{bmatrix} i\omega_n-\epsilon_+ +i\Gamma\,\mathrm{sgn}(\omega_n) & 0 \\ 0 & i\omega_n-\epsilon_- +i\Gamma\,\mathrm{sgn}(\omega_n) \end{bmatrix} \tag{13}$$

and

$$\hat{A}(\mathbf{k};\omega)=\begin{bmatrix} \dfrac{2\Gamma}{(\omega-\epsilon_+)^2+\Gamma^2} & 0 \\ 0 & \dfrac{2\Gamma}{(\omega-\epsilon_-)^2+\Gamma^2}. \end{bmatrix} \tag{14}$$

The diagonal elements of the spectral function can be interpreted as the density of electronic states in the bands.

## III. PLANE-CHAIN MODEL

In this section we describe a simple model containing a plane layer and a chain layer. The model is meant to incorporate the most important features of the chain-plane coupling in $YBCO_{7-\delta}$. In the discussion which follows, it will be made clear that the interband terms in the optical conductivity (which are important for $\sigma_{zz}$) are sensitive to the specifics of the band structure, which we cannot hope to describe correctly with our model. However, we will still be able to draw a number of general conclusions which should apply to models with a more accurate description of the unit cell.

For this work we will take the dispersion in the plane layer to be

$$\xi_1=-2t_1[\cos(k_xa)+\cos(k_ya)-2B\cos(k_xa)\cos(k_ya)] -\mu_1, \tag{15a}$$

and the dispersion in the chain layer to be

$$\xi_2=-2t_2\cos(k_ya)-\mu_2, \tag{15b}$$

where $a$ is the lattice constant in the $a$ (or equivalently $x$) and $b$ (or $y$) directions. There have been a number of attempts to fit the Fermi surface of the plane layer either to band structure calculations[23–25] or to angle-resolved photoemission experiments;[26] however, we are unaware of any work that attempts to find a phenomenological chain Fermi surface. In any case, a more accurate Fermi surface will not affect our basic (qualitative) conclusions, although the quantitative results of our calculations are quite sensitive to the band structure.

The simplest model of interlayer coupling is

$$t=-2t_\perp\cos(k_zd/2), \tag{15c}$$

where $d$ is the lattice constant in the $c$ (or $z$) direction. The form of Eq. (15c) makes the assumption that we have *coherent* single electron transport along the $c$ axis.

There have been many models of incoherent transport between layers.[4–9] A review of some of the models has been provided by Cooper and Gray.[1] As these models are not directly relevant to our present work, it will be sufficient here to provide a few highlights. In the work of Graf *et al.*,[4] no contribution from coherent transport is envisaged (i.e., $t_\perp = 0$) and the $c$-axis transport proceeds entirely through incoherent elastic scattering. In this case, the resistivity along $c$ is inversely proportional to that in the $ab$ plane. On the other hand, Kumar and Jayannavar[7] envisage tunneling between layers but in the limit that the tunneling time is larger than the in-plane scattering time. The effective transverse tunneling matrix element is modulated and reduced by the in-plane scattering and the $c$-axis conductivity becomes proportional to the $a$-$b$ plane scattering time. Leggett[8] envisages thermal depairing between layers for the case $t_\perp < k_B T$ while Anderson and Zou[9] consider the possibility that the $CuO_2$ planes cannot be described in Fermi liquid theory and involve spin and charge separation. This implies blocking of $c$-axis transport. Finally, Rojo and Levin[6] consider the possibility that $c$-axis transport proceeds through the combination of $t_\perp$ and incoherent transport due to elastic (impurity) and inelastic (phonon) assisted processes.

Here only the coherent contribution is included. It should also be remembered that we have oversimplified the internal structure of the unit cell in YBCO, particularly since we have only included one type of hopping mechanism which is paramatrized by $t_\perp$. In reality, there could be several types of hopping process occurring. For example, the coupling between planes and chains could be coherent while the intercell coupling could be incoherent. These issues are not treated here and go beyond the scope of our work. They are mentioned, however, so that the reader understands clearly the limitations of our work. We do feel, however, that near optimal doping YBCO is one of the few materials to display coherent transport between layers, and that our description of the interlayer coupling is reasonable.

The vertex functions are

$$\gamma_x(\mathbf{k},\mathbf{k}) = \begin{bmatrix} v_{1x} & 0 \\ 0 & 0 \end{bmatrix}, \tag{16a}$$

$$\gamma_y(\mathbf{k},\mathbf{k}) = \begin{bmatrix} v_{1y} & 0 \\ 0 & v_{2y} \end{bmatrix}, \tag{16b}$$

and

$$\gamma_z(\mathbf{k},\mathbf{k}) = \begin{bmatrix} 0 & v_\perp \\ v_\perp & 0 \end{bmatrix}, \tag{16c}$$

where $v_{i\mu} = \hbar^{-1}\partial\xi_i/\partial k_\mu$ and $v_\perp = \hbar^{-1}\partial t/\partial k_z$.

The change of basis is simple to perform and

$$\hat{\gamma}_x(\mathbf{k},\mathbf{k}) = \frac{v_{1x}}{\epsilon_+ - \epsilon_-}\begin{bmatrix} \xi_1 - \epsilon_- & t \\ t & \epsilon_+ - \xi_1 \end{bmatrix}, \tag{17a}$$

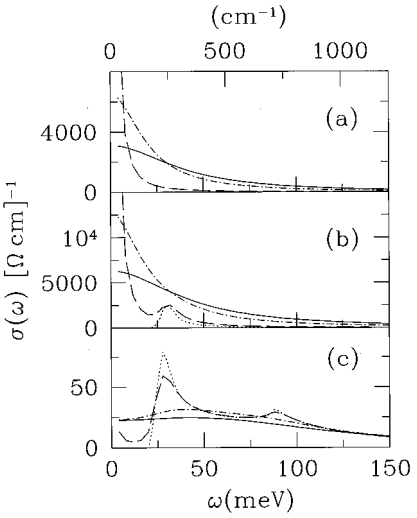


FIG. 2. Normal state optical conductivity in the (a) $x$, (b) $y$, and (c) $z$ directions for the plane-chain model. The conductivity is shown for temperatures 200 K (solid curve), 100 K (dot-dashed curve), 10 K (dashed curve), and 0 K (dotted curve). The scattering rate is $1/\tau = 20$ meV at 100 K and it scales linearly with temperature. The conductivity in the $z$ direction is dominated by interband processes and has a non-Drude appearance, while the conductivity in the $x$ and $y$ directions has a predominantly Drude-like behavior, although there is a small interband contribution to $\sigma_{yy}$. The band structure parameters are the same as in Fig. 1, except that $t_\perp = 5$ meV.

$$\hat{\gamma}_y(\mathbf{k},\mathbf{k}) = \frac{v_{1y}}{\epsilon_+ - \epsilon_-}\begin{bmatrix} \xi_1 - \epsilon_- & t \\ t & \epsilon_+ - \xi_1 \end{bmatrix} + \frac{v_{2y}}{\epsilon_+ - \epsilon_-}\begin{bmatrix} \xi_2 - \epsilon_- & t \\ t & \epsilon_+ - \xi_2 \end{bmatrix}, \tag{17b}$$

and

$$\hat{\gamma}_z(\mathbf{k},\mathbf{k}) = \frac{v_\perp}{\epsilon_+ - \epsilon_-}\begin{bmatrix} 2t & \xi_2 - \xi_1 \\ \xi_2 - \xi_1 & 2t \end{bmatrix}. \tag{17c}$$

In the derivation of Eqs. (17), use was made of the fact that $t(\mathbf{k}) \geqslant 0$. We are now able to evaluate the real part of the conductivity tensor [Eq. (12)] using Eqs. (14) and (17).

In Fig. 2 the conductivity is plotted as a function of frequency for a number of different temperatures. The strength of the interlayer coupling is relatively weak ($t_\perp = 5$ meV) and this is reflected in the small magnitude of the $c$-axis conductivity. We point out that the case presented in Fig. 2 provides a qualitative description of what is observed in underdoped $YBCO_{6.7}$.[11,12] To begin with, the conductivity in the $a$ direction has a traditional Drude-like structure. Since the scattering rate scales linearly with temperature, the width of the Drude-peak also scales linearly with temperature, and at $T = 0$, the conductivity is a $\delta$ function at $\omega = 0$. The conductivity in the $b$ direction also has a predominantly Drude-like structure but its magnitude is roughly twice that of $\sigma_{xx}$. This is because there are two current-carrying channels in the $b$ direction (the chains and the planes) and only one in the $a$ direction (the planes). At low temperatures there is a small non-Drude contribution due to interband transitions

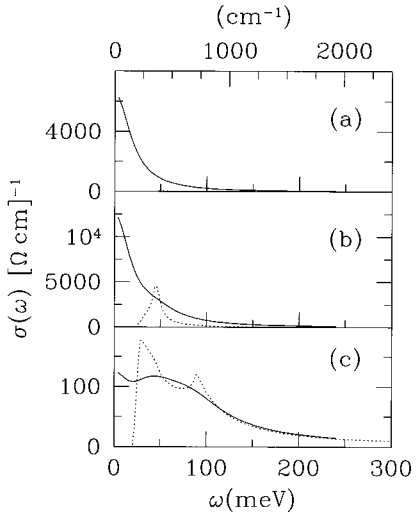


FIG. 3. The normal state conductivity is shown for the (a) $x$, (b) $y$, and (c) $z$ directions at 100 K (solid curve) and 0 K (dotted curve). The band structure differs from that of Fig. 2 by the magnitude of the chain-plane coupling, which is $t_\perp = 10$ meV here.

which becomes visible, and at $T=0$, the interband transitions are the only mechanism for conductivity at finite frequency.

In contrast with $\sigma_{xx}(\omega)$ and $\sigma_{yy}(\omega)$, the conductivity in the $c$ direction has a decidedly non-Drude behavior and, instead, appears as a broad background. As we shall see, this is entirely due to interband transitions between the plane and chain layers. A further, interesting feature in $\sigma_{zz}(\omega)$ is that at high temperatures there is very little structure as a function of frequency $\omega$, but that structure appears at low temperatures. This can be attributed to the linear decrease in the scattering rate with temperature assumed in our work; at high temperature the large scattering rate smears out the structure in $\sigma_{zz}(\omega)$. Perhaps the most striking feature in $\sigma_{zz}$ is the development of a gap as the temperature is lowered. This gap

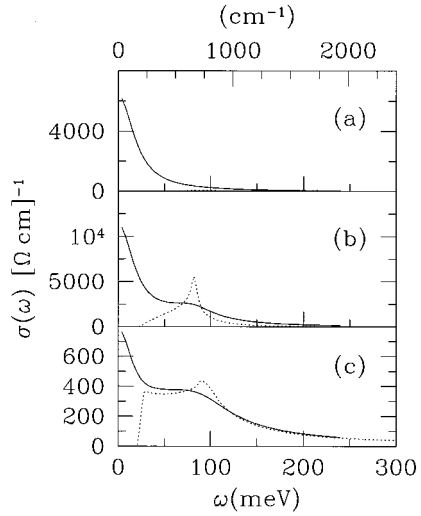


FIG. 4. The normal state conductivity is shown, as in Fig. 3, but with $t_\perp = 20$ meV. The conductivity in the $z$ direction has a significant Drude part, while the conductivity in the $y$ direction has a significant interband part.

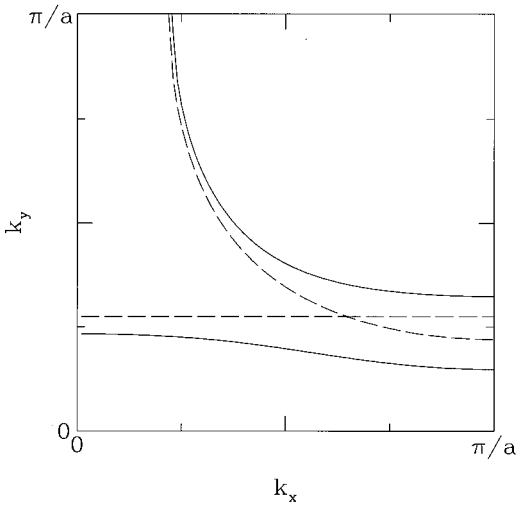


FIG. 5. The Fermi surface is shown for the chain-plane model for a case where the chain and plane Fermi surfaces (dashed curves) cross. This case is qualitatively different from the case shown in Fig. 1 because there is no band gap. As a result, a pseudogap is not expected in the $c$-axis optical conductivity. The band structure parameters chosen for this case are $\{t_1,t_2,\mu_1,\mu_2,t_\perp\} = \{70,100,-65,-130,20\}$ meV and $B=0.45$.

is just the gap between the two bands $\epsilon_+$ and $\epsilon_-$, and at high temperatures it is filled in by the large scattering rate $\Gamma$.

In Figs. 3 and 4, the optical conductivity is plotted for larger values of the chain-plane coupling $t_\perp$. The larger cou-

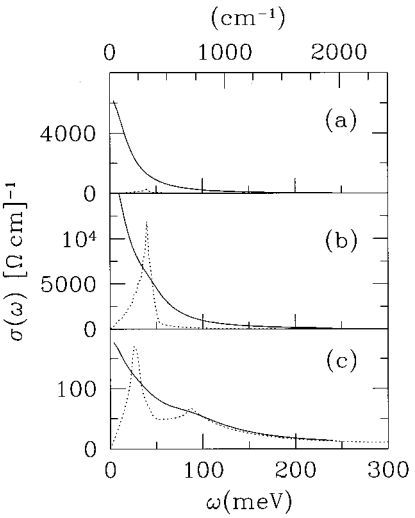


FIG. 6. The optical conductivity is shown along the (a) $x$, (b) $y$, and (c) $z$ directions at $T=100$ K and at $T=0$ K. The $T=0$ K optical conductivity is entirely due to interband transitions at finite frequencies. In $\sigma_{xx}$ there is only a very small interband contribution, while in $\sigma_{yy}$ and $\sigma_{zz}$, the interband contributions are substantial. At $T=100$ K, however, it is difficult to distinguish the interband contribution from the Drude contribution because of the large scattering rate. There is also a large Drude contribution to $\sigma_{zz}$ and there is no pseudogap, although the interband conductivity still falls to zero linearly with $\omega$. The band parameters are the same as in Fig. 5, except that $t_\perp = 10$ meV.

pling has almost no effect on $\sigma_{xx}$. On the other hand, the larger coupling enhances the role of interband transitions in $\sigma_{yy}$, and also increases the Drude (or intraband) contribution to $\sigma_{zz}$. Note that the Drude peak at low $\omega$ is not seen in $\sigma_{zz}$ in Fig. 2 where $t_\perp$ is small, while in Fig. 4, where $t_\perp$ is much larger, the Drude peak is seen as a sharp turn upward at low $\omega$.

The conductivities shown in Figs. 3 and 4 are not quite appropriate to describe optimally doped YBCO even though the magnitudes of the conductivities are approximately right. This is because there is still a gap in the conductivity at low temperatures. However, by shifting the chain Fermi surface slightly, as shown in Fig. 5, we are able to eliminate the band gap. It is very plausible that a change in doping will change the structure of the chain and plane Fermi surfaces so that they cross. In Figs. 6 and 7 the conductivity is shown at $T=100$ K and at $T=0$ K for $t_\perp=10$ meV and 20 meV, respectively. In Fig. 6, the conductivity has a Drude-like appearance in both the $a$ and $b$ directions, even though there is a large interband contribution to $\sigma_{yy}$. The interband contribution can be resolved in $\sigma_{yy}$ if the temperature (and therefore the scattering rate) is reduced. Unfortunately, this is difficult to do experimentally because of the onset of superconductivity near 100 K. In both Figs. 6 and 7, the $c$-axis response shows a Drude-like peak at low $\omega$ and high temperature (solid curve). On closer examination, the response is a combination of a Drude and flat interband contribution. As the temperature is lowered, this second contribution remains (dotted curve) and a pseudogap at low $\omega$ is resolved (i.e., the conductivity is depressed but goes strictly to zero only at $\omega=0$).

## IV. CLEAN LIMIT

The purpose of this section is to understand the role of interband transitions a little better. We will examine why it is that the interband transitions are most important in the $c$-axis conductivity for small interlayer coupling, while they are most important for the $b$-axis conductivity for large interlayer coupling, and are never important for the $a$-axis conductivity. Finally, we shall derive expressions for the intraband and interband conductivities in the clean ($\Gamma=0$) limit and show how $\sigma_{zz}(\omega)$ can be interpreted as a probe of the band structure.

Let us start by writing out Eq. (12), the formula for the conductivity, explicitly:

$$\mathrm{Re}[\sigma_{\mu\mu}(\omega)]=\frac{e^2\hbar}{2\pi\Omega}\sum_{\mathbf{k}}\int_{-\infty}^{\infty}dx\{\hat{A}_{11}(\mathbf{k};x)\hat{A}_{11}(\mathbf{k};x+\hbar\omega)[\hat{\gamma}_{11}]_\mu^2+\hat{A}_{22}(\mathbf{k};x)\hat{A}_{22}(\mathbf{k};x+\hbar\omega)[\hat{\gamma}_{22}]_\mu^2+[\hat{A}_{11}(\mathbf{k};x)\hat{A}_{22}(\mathbf{k};x+\hbar\omega)$$
$$+\hat{A}_{22}(\mathbf{k};x)\hat{A}_{11}(\mathbf{k};x+\hbar\omega)][\hat{\gamma}_{12}]_\mu[\hat{\gamma}_{21}]_\mu\}\frac{f(x)-f(x+\hbar\omega)}{\hbar\omega}. \tag{18}$$

The first two terms in the integrand describe *intraband* processes and yield Drude-like behavior. This fact can be made clear if we remark that

$$[\hat{\gamma}_{ij}]_\mu=\frac{\delta_{ij}}{\hbar}\frac{\partial\epsilon_i}{\partial k_\mu}+\frac{1}{\hbar}[\epsilon_i-\epsilon_j]\left[U^\dagger(\mathbf{k})\frac{\partial U(\mathbf{k})}{\partial k_\mu}\right]_{ij} \tag{19}$$

(where we use the notation $\epsilon_1\equiv\epsilon_+$ and $\epsilon_2\equiv\epsilon_-$), so that the first two terms in the conductivity are

$$\sigma_{\mathrm{Drude}}(\omega)=\frac{e^2\hbar}{2\pi\Omega}\sum_{\pm}\sum_{\mathbf{k}}\int_{-\infty}^{\infty}dx\left[\frac{1}{\hbar}\frac{\partial\epsilon_\pm}{\partial k_\mu}\right]^2\frac{2\Gamma}{(x-\epsilon_\pm)^2+\Gamma^2}\frac{2\Gamma}{(\hbar\omega+x-\epsilon_\pm)^2+\Gamma^2}\frac{f(x)-f(x+\hbar\omega)}{\hbar\omega}. \tag{20}$$

In the simple case of a single-band system with a spherical Fermi surface, this becomes the usual expression for the optical conductivity,

$$\sigma(\omega)=2e^2N(0)\frac{v_F^2}{3}\frac{\tau}{1+\omega^2\tau^2},$$

where $\Gamma=\hbar/2\tau$.

In the clean limit ($\Gamma\to0$),

$$\frac{\Gamma}{x^2+\Gamma^2}\to\pi\delta(x).$$

and the intraband conductivity becomes

$$\sigma_{\mathrm{Drude}}(\omega)=-\frac{2\pi e^2\hbar}{\Omega}\sum_{\pm}\sum_{\mathbf{k}}\left[\frac{1}{\hbar}\frac{\partial\epsilon_\pm}{\partial k_\mu}\right]^2\frac{\partial f(\epsilon_\pm)}{\partial\epsilon_\pm}\delta(\hbar\omega). \tag{21}$$

The Drude peak in the conductivity is now a $\delta$ function centered at $\omega=0$.

The remaining terms in Eq. (18) are the *interband* terms. In the clean limit the interband contribution is (for $\omega>0$)

$$\sigma_{\mathrm{Inter}}(\omega)=\frac{2\pi e^2\hbar}{\Omega}\sum_{\mathbf{k}}[\hat{\gamma}_{12}]_\mu^2\frac{f(\epsilon_-)-f(\epsilon_+)}{\epsilon_+-\epsilon_-}$$
$$\times\delta(\hbar\omega-\epsilon_++\epsilon_-). \tag{22}$$

In order to get some sense of the relative magnitudes of $\sigma_{\mathrm{Drude}}(\omega)$ and $\sigma_{\mathrm{Inter}}(\omega)$ we compare the magnitudes of

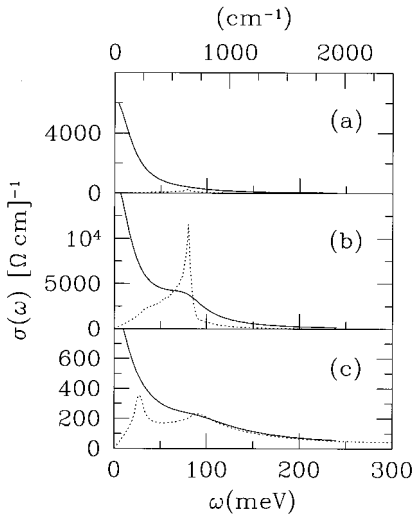


FIG. 7. The optical conductivity is shown, as in Fig. 6, but with $t_\perp = 20$ meV.

$[\hbar^{-1}\partial\epsilon_\pm/\partial k_\mu]^2$ and $[\gamma_{12}]_\mu^2$. In the analysis which follows, we will compare these two quantities for $\sigma_{xx}$, $\sigma_{yy}$ and $\sigma_{zz}$.

In the $x$ direction,

$$\left[\frac{1}{\hbar}\frac{\partial\epsilon_\pm}{\partial k_x}\right]^2 = \left[v_{1x}\frac{\xi_1 - \epsilon_\mp}{\epsilon_+ - \epsilon_-}\right]^2$$

and

$$[\hat{\gamma}_{12}]_x^2 = \left[v_{1x}\frac{t}{\epsilon_+ - \epsilon_-}\right]^2.$$

Throughout most of the Brillouin zone, $|\xi_1 - \xi_2| \gg 2|t|$ and

$$\epsilon_+ \sim \max(\xi_1, \xi_2) + \frac{t^2}{(\xi_1 - \xi_2)^2},$$

$$\epsilon_- \sim \min(\xi_1, \xi_2) - \frac{t^2}{(\xi_1 - \xi_2)^2},$$

from which it follows that the largest contribution to $\sigma_{\text{Drude}}(\omega)$ will be of the order $v_{1x}^2[1 + O(t^2/(\xi_1 - \xi_2)^2)]$, where the correction term is of the order 1/25 throughout most of the Brillouin zone. In the same way, we can immediately see that throughout most of the Brillouin zone, the interband contribution to $\sigma_{xx}$ will be $v_{1x}^2[O(t^2/(\xi_1 - \xi_2)^2)]$. Of course, in the region of the Brillouin zone where the chain and plane Fermi surfaces are close together, the above argument does not hold. However, the value of $v_{1x}$ is small in this region of the Brillouin zone and we conclude that interband processes do not make a significant contribution to $\sigma_{xx}$.

Much of the above argument holds for $\sigma_{yy}$ as well, and we can conclude that throughout most of the Brillouin zone, interband processes are unimportant. Unlike the case of $\sigma_{xx}$, however, $v_{1y}$ and $v_{2y}$ are not small in regions of the Brillouin zone where interband transitions are significant, and there will therefore be small but noticeable non-Drude contribution to the $b$-axis conductivity.

The situation is somewhat reversed for the $c$-axis conductivity, where we can show that interband processes play a dominant role. In the $z$ direction,

$$\left[\frac{1}{\hbar}\frac{\partial\epsilon_\pm}{\partial k_z}\right]^2 = \left[v_\perp\frac{2t}{\epsilon_+ - \epsilon_-}\right]^2$$

and

$$[\hat{\gamma}_{12}]_z^2 = \left[v_\perp\frac{\xi_1 - \xi_2}{\epsilon_+ - \epsilon_-}\right]^2.$$

Inspection of these two equations shows that while the interband contribution still scales as $t_\perp^2$ (through the factor of $v_\perp$), the Drude component now scales as $t_\perp^4$. In other words, Drude contribution to the conductivity is smaller than the interband contribution by a factor $t^2/(\xi_1 - \xi_2)^2$.

In summary, then, the conductivities scale with $t_\perp$ as follows: For $\sigma_{xx}$ and $\sigma_{yy}$, we find that the Drude part scales as $(t_\perp)^0$ and the interband part scales as $t_\perp^2$ while for $\sigma_{zz}$ the interband part scales as $t_\perp^2$ and the Drude part as $t_\perp^4$.

We will finish this section with a brief mention of the usefulness of $\sigma_{zz}$ as a probe of the band structure. The factor $\delta(\hbar\omega - \epsilon_+ + \epsilon_-)$ in Eq. (22) means that the interband conductivity is a probe of the *joint density of states* of the two bands. The sum in Eq. (22) is weighted by the thermal factor $f(\epsilon_-) - f(\epsilon_+)$, which restricts the transitions to be between filled and empty states. At zero temperature, this term restricts the sum to lie in regions of the Brillouin zone where $\epsilon_+\epsilon_- < 0$ [i.e., $\epsilon_-(\mathbf{k})$ is a filled state and $\epsilon_+(\mathbf{k})$ is an empty state]. In Fig. 1, this means that the interband transitions occur in the area contained by the two Fermi surface curves. The constant energy-difference contours are also shown in Fig. 1 as the dotted lines.

When we compare the chain-plane system with the bilayer model in the next section, we will see that the chain-plane system is somewhat special in that the joint density of states is spread over a broad range of energies. In simple terms, the interband contribution to the $c$-axis conductivity exists over an energy scale of 1 eV because the chain and plane bands have such different structure, and the energy difference $\epsilon_+(\mathbf{k}) - \epsilon_-(\mathbf{k})$ takes on all different values on the energy scale of 1 eV in the Brillouin zone. In the bilayer system, however, where the two layers are identical, the energy difference is restricted to a narrow range of values, and the interband contribution to the optical conductivity will result in a narrow peak.

## V. BILAYER MODEL

In this model, we have two planes per unit cell. The planes have equivalent band structures, but are made inequivalent by their spacing. In other words, the planes are alternately spaced by distances $d_1$ and $d_2$ along the $c$ axis, where $d_1 + d_2 = d$ is the unit cell length. In the special case $d_1 = d_2$, the model reduces to a single-band model as we shall show below.

The energy dispersion in the planes is $\xi_1 = \xi_2 = \xi$. For our

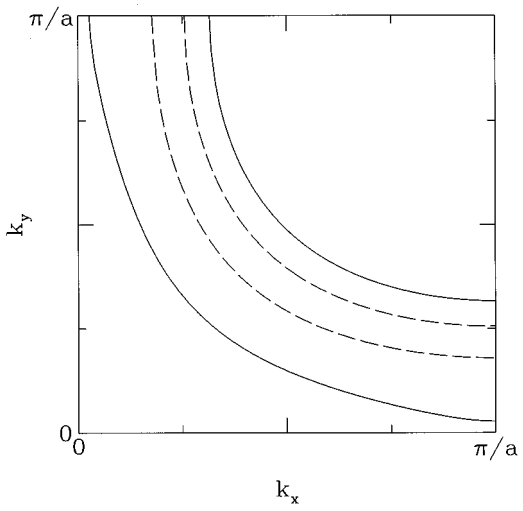


FIG. 8. The Fermi surface is shown for the bilayer system. In this model, there are two plane layers per unit cell. The dispersions in the layers are the same, but they are spaced distances $d_1$ and $d_2$ apart in alternating fashion. The Fermi surfaces are shown for $k_z=0$ (solid line) and $k_z=\pi/d$ (dashed line). The minimum and maximum coupling strengths are $2|t_{\perp 1}-t_{\perp 2}|$ and $2|t_{\perp 1}+t_{\perp 2}|$, respectively. The model parameters are $\{t_1,\mu_1,t_{\perp 1},t_{\perp 2}\}=\{70,-65,20,10\}$meV, $d_1=0.3d$, and $B=0.45$.

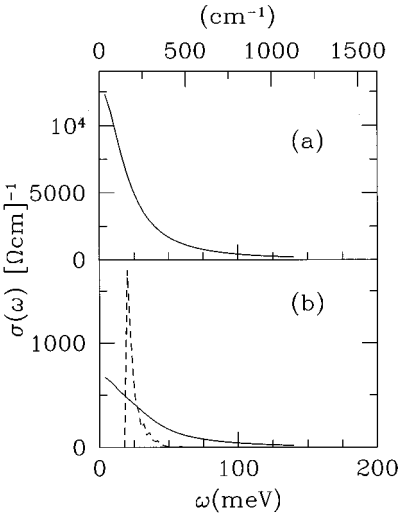


FIG. 9. The optical conductivity is shown for the bilayer system (a) in the $a$ and $b$ directions and (b) in the $c$ direction. The conductivity is shown at $T=100$ K (solid curve) and at $T=0$ K (dotted curve). The in-plane conductivity has a Drude shape, while the $c$ axis conductivity has a large interband contribution. At $T=0$ K, the in-plane conductivity vanishes at finite frequency. Along the $c$ axis, however, the interband contribution remains for frequencies $2|t_{\perp 1}-t_{\perp 2}|\leq\hbar\omega\leq 2|t_{\perp 1}+t_{\perp 2}|$. The model parameters are the same as those in Fig. 8.

numerical calculations, we will take

$$\xi=-2t_1[\cos(k_x a)+\cos(k_y a)-2B\cos(k_x a)\cos(k_y a)]-\mu_1. \tag{23a}$$

In this section, we will also calculate the conductivity analytically using the simpler band structure

$$\xi=\frac{\hbar^2}{2m}(k_\parallel^2-k_F^2) \tag{23b}$$

where $v_F$ is the Fermi velocity at the (circular) Fermi surface, $k_\parallel=\sqrt{k_x^2+k_y^2}$, and $k_F$ is the value of $k_\parallel$ at the Fermi surface.

The interlayer coupling term takes the form[19]

$$t(\mathbf{k})=t_{\perp 1}e^{ik_z d_1}+t_{\perp 2}e^{-ik_z d_2}, \tag{23c}$$

where we expect that if $d_1<d_2$, then $t_{\perp 1}>t_{\perp 2}$. If $d_1=d_2$ and $t_1=t_2$, then $t(\mathbf{k})$ reduces to Eq. (15c). The band energies are

$$\epsilon_\pm=\xi(\mathbf{k})\pm|t(\mathbf{k})|, \tag{24}$$

and the Fermi surface is shown in Fig. 8 for the case where $\xi$ is given by Eq. (23a). In the biplanar model, the bands are split by $2|t(\mathbf{k})|$ so that the maximum band energy difference is $2|t_{\perp 1}+t_{\perp 2}|$ and the minimum band energy difference is $2|t_{\perp 1}-t_{\perp 2}|$. Since $t_{\perp 1}$ and $t_{\perp 2}$ are typically much smaller than the bandwidths, this means that the interband contribution to $\sigma_{zz}$ will be over a small range of energies. As we will see from our numerical work, the bilayer is not a likely source for the broad, experimentally observed, $c$-axis response.

The unitary matrix which diagonalizes the Hamiltonian is now

$$U(\mathbf{k})=\frac{1}{\sqrt{2}|t|}\begin{bmatrix}-t & -t\\ -|t| & |t|\end{bmatrix}. \tag{25}$$

The vertex function for the in-plane conductivity $\sigma_{xx}$ is

$$\hat{\gamma}_x(\mathbf{k},\mathbf{k})=\gamma_x(\mathbf{k},\mathbf{k})=\begin{bmatrix}v_x & 0\\ 0 & v_x\end{bmatrix}, \tag{26}$$

where $v_x=\hbar^{-1}\partial\xi/\partial k_x$. We can see that there will be no interband contribution to $\sigma_{xx}(\omega)$ since $\hat{\gamma}_x$ has no off-diagonal matrix elements. In fact, Eq. (12) becomes

$$\mathrm{Re}[\sigma_{xx}(\omega)]=\frac{e^2\hbar}{2\pi\Omega}\sum_{\pm}\sum_{\mathbf{k}}\int_{-\infty}^{\infty}dx v_x^2\frac{f(x)-f(x+\hbar\omega)}{\hbar\omega}\times\frac{2\Gamma}{(x-\epsilon_\pm)^2+\Gamma^2}\frac{2\Gamma}{(x+\hbar\omega-\epsilon_\pm)^2+\Gamma^2}. \tag{27}$$

If we take $\xi$ from Eq. (23b), then we get, in the usual way, the Drude conductivity

$$\mathrm{Re}[\sigma_{xx}]=\frac{4e^2\hbar N_\parallel}{d}\frac{v_F^2}{2}\frac{\tau}{\omega^2\tau^2+1}, \tag{28}$$

where $N_\parallel$ is the two dimensional density of states for a single layer. In three dimensions, with a cylindrical Fermi surface, the density of states for the bilayer is $N=2N_\parallel/d$. Numerical calculations of the optical conductivity, shown in Fig. 9, are in qualitative agreement with Eq. (28).

The vertex function for the conductivity along the $c$ axis is

$$\hat{\gamma}_z(\mathbf{k},\mathbf{k}) = U^\dagger(\mathbf{k}) \begin{bmatrix} 0 & v_\perp \\ v_\perp^* & 0 \end{bmatrix} U(\mathbf{k}) = \frac{1}{|t|} \begin{bmatrix} \mathrm{Re}(v_z t^*) & -i\mathrm{Im}(v_z t^*) \\ i\mathrm{Im}(v_z t^*) & -\mathrm{Re}(v_z t^*) \end{bmatrix}, \tag{29}$$

where $v_z = \hbar^{-1}\partial t/\partial k_z$. The diagonal elements in $\hat{\gamma}_z$ are

$$\frac{\mathrm{Re}(v_z t^*)}{|t|} = \frac{1}{\hbar}\frac{\partial |t|}{\partial k_z} = \frac{1}{\hbar}\frac{t_{\perp 1} t_{\perp 2}}{|t|} d \sin(k_z d) \leqslant \frac{1}{\hbar}\min(t_{\perp 1}, t_{\perp 2}) d \sin(k_z d),$$

so that the intraband (or Drude) conductivity is limited by the lessor of $t_{\perp 1}$ and $t_{\perp 2}$. In other words the Drude current is limited by the weak link along the $c$ axis. The off-diagonal elements in $\hat{\gamma}_z$ are

$$\frac{\mathrm{Im}(v_z t^*)}{|t|} = \frac{1}{\hbar}[t_{\perp 1}^2 d_1 - t_{\perp 2}^2 d_2 + t_{\perp 1} t_{\perp 2}(d_1 - d_2)\cos(k_z d)]/|t|, \tag{30}$$

which vanishes when $t_1 = t_2$ and $d_1 = d_2$. Unlike the intraband conductivity, the interband conductivity does not become small as either $t_{\perp 1}$ or $t_{\perp 2}$ vanishes. In other words, the interband contribution to $\sigma_{zz}$ persists even in the limit that the bilayers become isolated from their neighbors.

The conductivity along the $c$ axis is

$$\mathrm{Re}[\sigma_{zz}(\omega)] = \frac{e^2\hbar}{2\pi\Omega}\sum_{\mathbf{k}} \int_{-\infty}^{\infty} dx \frac{f(x) - f(x+\hbar\omega)}{\hbar\omega} \left\{ \sum_{\pm} \frac{2\Gamma}{(x-\epsilon_\pm)^2+\Gamma^2} \frac{2\Gamma}{(x+\hbar\omega-\epsilon_\pm)^2+\Gamma^2} \left[\frac{\mathrm{Re}[v_z t^*]}{|t|}\right]^2 + \sum_{\pm} \frac{2\Gamma}{(x-\epsilon_\pm)^2+\Gamma^2} \frac{2\Gamma}{(x+\hbar\omega-\epsilon_\mp)^2+\Gamma^2} \left[\frac{\mathrm{Im}[v_z t^*]}{|t|}\right]^2 \right\}. \tag{31}$$

The first term in the curly brackets gives the intraband conductivity while the second gives the interband conductivity. We can proceed further if we take $\xi$ to be of the form given in Eq. (23b). Then we find that

$$\mathrm{Re}[\sigma_{zz}(\omega)] = \frac{2e^2 N_\parallel}{d} \left\{ 2\frac{\tau}{\omega^2\tau^2+1} \left\langle \left[\frac{\mathrm{Re}[v_z t^*]}{|t|}\right]^2 \right\rangle_{k_z} + \sum_{\pm} \left\langle \frac{\tau}{\tau^2(\omega \pm 2|t|/\hbar)^2+1} \left[\frac{\mathrm{Im}[v_z t^*]}{|t|}\right]^2 \right\rangle_{k_z} \right\}, \tag{32}$$

where $\langle \cdots \rangle_{k_z}$ denotes an average over $k_z$.

The first term in Eq. (32) has the usual Drude frequency dependence, weighted by an average Fermi velocity. The second term is the interband term. Its frequency dependence is an average over $k_z$ of Lorentzians centered at $\hbar\omega = 2|t(k_z)|$. This is what is seen in Fig. 9. In the limit that we have a single bilayer ($t_{\perp 2} \to 0$), $|t(k_z)| \to t_{\perp 1}$ and

$$\mathrm{Re}[\sigma_{zz}(\omega)] \to \frac{2e^2 N_\parallel t_{\perp 1}^2 d_1^2}{\hbar^2 d} \frac{\tau}{\tau^2(\omega - 2t_{\perp 1}/\hbar)^2+1}. \tag{33}$$

The $c$-axis response becomes a Lorentzian centered at $\hbar\omega = 2t_{\perp 1}$. This case has been studied in detail by Gartstein, Rice, and van der Marel.[27]

## VI. SUM RULES

In this section we will discuss the partial sum rule for the conductivity within our model. The full sum rule

$$\frac{\pi n e^2}{2m} = \int_0^\infty d\omega \sigma(\omega), \tag{34}$$

where $n$ is the electron density and $m$ is the bare mass, is well known. Equation (34) is often used as a means of measuring the electron density in the cuprate superconductors.

In any practical evaluation of Eq. (34), it is necessary to impose a cutoff in the frequency integration, and often this cutoff is taken to be below the onset of interband transitions in the $a$ and $b$ directions, so that only the Drude-like response is counted. If we define, therefore, a plasma frequency tensor by

$$\frac{\omega_p^2}{8} = \int_0^\infty d\omega \sigma_{\mathrm{Drude}}(\omega) \tag{35}$$

and consider $\Gamma \to 0$ for simplicity, then, from Eq. (21),

$$\frac{\omega_{p\mu\nu}^2}{8} = -\frac{\pi e^2}{\Omega}\sum_{\pm}\sum_{\mathbf{k}} \left[\frac{1}{\hbar^2}\frac{\partial \epsilon_\pm}{\partial k_\mu}\frac{\partial \epsilon_\pm}{\partial k_\nu}\right] \frac{\partial f(\epsilon_\pm)}{\partial \epsilon_\pm}. \tag{36}$$

Integrating by parts in $k_\mu$ gives

$$\frac{\omega_{p\mu\nu}^2}{8} = \frac{\pi e^2}{\Omega}\sum_{\pm}\sum_{\mathbf{k}} \left[\frac{1}{\hbar^2}\frac{\partial^2 \epsilon_\pm}{\partial k_\mu \partial k_\nu}\right] f(\epsilon_\pm). \tag{37}$$

Now, we can define an average effective mass tensor for each of the bands by

$$\overline{M_{\pm\mu\nu}^{-1}} = \frac{1}{n_\pm} \times \frac{2}{\Omega}\sum_{\mathbf{k}} \left[\frac{1}{\hbar^2}\frac{\partial^2 \epsilon_\pm}{\partial k_\mu \partial k_\nu}\right] f(\epsilon_\pm), \tag{38}$$

where

$$n_\pm = \frac{2}{\Omega}\sum_{\mathbf{k}} f(\epsilon_\pm), \tag{39}$$

so that

$$\omega_{p\mu\nu}^2 = 4\pi e^2 \sum_{\pm} n_{\pm} \overline{M_{\pm\mu\nu}^{-1}}. \tag{40}$$

We emphasize here that $\overline{M_{\pm\mu\nu}^{-1}}$ is an average of the effective mass tensor *over all filled states*, and is not just the effective mass tensor at the Fermi surface. As a result of this, $\overline{M_{\pm\mu\nu}^{-1}}$ depends on the filling of the bands. For this reason, we suggest that it may actually be difficult to determine changes in the electron density with doping in the high-$T_c$ materials.

## VII. CONCLUSION AND DISCUSSION

We have calculated the optical conductivity for a simple layered model of $YBCO_{7-\delta}$, in which each unit cell consists of a two-dimensional plane layer and a one-dimensional chain layer. The model contains two important pieces of physics. First, we assumed that the layers are coherently coupled and measured the strength of the coupling with the parameter $t_\perp$. As we mentioned earlier, this is different from the more usual point of view which ascribes the broad background and absence of a Drude peak in the $c$-axis conductivity to incoherent $c$-axis transport. The second important piece of physics is the scattering rate $\Gamma$, which was assumed to vary linearly with $T$.

In a multilayer system, we found that there are two contributions to the optical conductivity: intraband and interband. For the in-plane conductivity ($\sigma_{xx}$ and $\sigma_{yy}$) we found that the intraband conductivity dominates the response, resulting in Drude-like conductivities. In fact, we showed that the intraband terms scale as $(t_\perp)^0$, while the interband terms scale as $t_\perp^2$ for small $t_\perp$. On the other hand, we found that the $c$-axis response is dominated by the interband contribution (which still scales as $t_\perp^2$) since the intraband contribution scales as $t_\perp^4$. For this reason, we found that the $c$-axis optical conductivity has a non-Drude appearance.

In the plane-chain model, the $\sigma_{zz}$ consists of a broad featureless response at high temperatures. As the temperature is lowered, structure develops in the conductivity. In some cases, we found that a pseudogaplike structure appeared. The broad range of frequencies spanned by $\sigma_{zz}$ is the result of the plane and chain bands having different geometries so that transitions between the two bands span a wide range of energies. In contrast, we showed that a bilayer system in which the two layers have identical band structures results in a $c$-axis conductivity which is finite only over a narrow range of frequencies.

The other feature of $\sigma_{zz}$—that structure appears as $T$ is lowered—is the result of having a temperature-dependent scattering rate. At $T=100$ K, for example, structure in $\sigma_{zz}$ is smeared out over 20 meV, while at $T=10$ K, structure can be resolved on a scale of 2 meV.

Finally, with this model, we have been able to comment on changes in $\sigma_{zz}$ with doping over the range $YBCO_{6.7}$ to $YBCO_7$. We have suggested that in slightly underdoped YBCO, there is a band gap between the plane and chain layers, which is reflected in a gap in the interband conductivity. Above a certain temperature, however, the band gap is hidden by the large scattering rate which smears out quasiparticle energies by more than the band gap. As the temperature is reduced, the quasiparticle energies become better defined and the band gap appears in the conductivity. The gap is similar in its appearance to the pseudogap observed in $YBCO_{6.7}$. At optimal doping, we have suggested that two changes must be made to the model. The first is that the strength of the chain-plane coupling must be increased—thus increasing the importance of the Drude contribution to $\sigma_{zz}$. The second is that the chain and plane Fermi surfaces must be made to cross, eliminating the pseudogap.

We point out that the exact shape of the interband contribution as a function of energy was found to be quite sensitive to details of the Fermi surfaces involved. This means that $c$-axis conductivity measurements could, in principle, be used to get information on the energy bands as well as on the filling factors for chains and planes and on their changes with oxygen doping.

While the sensitivity of the frequency dependence of $\sigma_c(\omega)$ to band structure could, in principle, be used to get spectroscopic information on electronic structure, it should be emphasized that the band structure used in our work is grossly oversimplified and so some of our detailed predictions cannot be applied directly to $YBa_2Cu_3O_x$. The qualitative features obtained and emphasized in this conclusion are, however, expected to be robust and remain in more complex models. Such calculations will need to employ more realistic band structures and, perhaps more importantly, consider the issue of intercell coupling which could be incoherent and quite different from the chain-plane hopping. Nevertheless, our model does exhibit many of the features observed in experiments on YBCO at optimum doping as well as underdoped and overdoped cases.

## ACKNOWLEDGMENTS

This work was supported by a Natural Sciences and Engineering Research Council of Canada (NSERC) grant, and by the Canadian Institute for Advanced Research (CIAR).

*Present address: Department of Physics, Indiana University, Swain Hall W 117, Bloomington, Indiana 47405.

[1] S.L. Cooper and K.E. Gray, in *Physical Properties of High Temperature Superconductors*, edited by D.M. Ginsberg (World Scientific, Singapore, 1994), Vol. IV, p. 62.

[2] Y. Iye, in *Physical Properties of High Temperature Superconductors*, edited by D.M. Ginsburg (World Scientific, Singapore, 1992), Vol. III, p. 285.

[3] J.M. Wheatley, T.C. Hsu, and P.W. Anderson, Phys. Rev. B **37**, 5897 (1988).

[4] M.J. Graf, D. Rainer, and J.A. Sauls, Phys. Rev. B **47**, 12 089 (1993).

[5] Y. Zha, S.L. Cooper, and D. Pines, Phys. Rev. B **53**, 8253 (1996).

[6] A.G. Rojo and K. Levin, Phys. Rev. B **48**, 16 861 (1993).

[7] N. Kumar and A.M. Jayannavar, Phys. Rev. B **45**, 5001 (1992).

[8] A.J. Leggett, Braz. J. Phys. **22**, 129 (1992).

[9] P.W. Anderson and Z. Zou, Phys. Rev. Lett. **60**, 132 (1988); **60**, 2557 (1988).

[10] T.A. Friedmann *et al.*, Phys. Rev. B **42**, 6217 (1990).

[11] C.C. Homes, T. Timusk, D.A. Bonn, R. Liang, and W.N. Hardy, Physica C **254**, 265 (1995).
[12] C.C. Homes, T. Timusk, R. Liang, D.A. Bonn, and W.N. Hardy, Phys. Rev. Lett. **71**, 1645 (1993).
[13] D.A. Bonn, S. Kamal, K. Zhang, R. Liang, and W.N. Hardy, J. Phys. Chem. Solids **56**, 1941 (1995).
[14] J.L. Tallon *et al.*, Phys. Rev. Lett. **74**, 1008 (1995).
[15] D.N. Basov *et al.*, Phys. Rev. Lett. **74**, 598 (1995).
[16] R. Gagnon, C. Lupien, and L. Taillefer, Phys. Rev. B **50**, 3458 (1994).
[17] K. Zhang *et al.*, Phys. Rev. Lett. **73**, 2484 (1994).
[18] G.D. Mahan, *Many-Particle Physics* (Plenum Press, New York, 1986), p. 695 ff.
[19] W.A. Atkinson and J.P. Carbotte, Phys. Rev. B **52**, 10 601 (1995).
[20] M. Tachiki, S. Takahashi, F. Steglich, and H. Adrian, Z. Phys. B **80**, 161 (1990); M. Tachiki, T. Koyama, and S. Takahashi, Prog. Theor. Phys. Suppl. **108**, 297 (1992); S. Takahashi and M. Tachiki, Physica C **170**, 505 (1990).
[21] A.Yu. Simonov, Physica C **211**, 455 (1993).
[22] J.E. Hirsch and F. Marsiglio, Phys. Rev. B **45**, 4807 (1992).
[23] O.K. Andersen, O. Jepsen, A.I. Liechtenstein, and I.I. Mazin, Phys. Rev. B **49**, 4145 (1995).
[24] W.E. Pickett, H. Krakauer, R.E. Cohen, and D.J. Singh, Science **255**, 46 (1992); W. E. Pickett, R.E. Cohen, and H. Krakauer, Phys. Rev. B **42**, 8764 (1990).
[25] J. Yu, S. Massida, A.J. Freeman, and D.D. Koelling, Phys. Lett. A **122**, 203 (1987).
[26] G. Blumberg, Branko P. Stojković, and M.V. Klein, Phys. Rev. B **52**, R15 741 (1995).
[27] Yu.N. Gartstein, M.J. Rice, and D. van der Marel, Phys. Rev. B **49**, 6360 (1994).